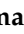*Article*

Energy Yield Assessment from Ocean Currents in the Insular Shelf of Cozumel Island

Juan Carlos Alcérreca-Huerta [1], Job Immanuel Encarnacion [2], Stephanie Ordoñez-Sánchez [2,*], Mariana Callejas-Jiménez [3] , Gabriel Gallegos Diez Barroso [3] , Matthew Allmark [4], Ismael Mariño-Tapia [5], Rodolfo Silva Casarín [6] , Tim O'Doherty [4] , Cameron Johnstone [2] and Laura Carrillo [3]

[1] Consejo Nacional de Ciencia y Tecnología-El Colegio de la Frontera Sur (CONACYT-ECOSUR), Department of Systematics and Aquatic Ecology, C.P 77014 Chetumal, Q. Roo, Mexico; jcalcerreca@conacyt.mx

[2] Energy Systems Research Unit, University of Strathclyde, Glasgow G1 1XJ, Scotland, UK; job.encarnacion@strath.ac.uk (J.I.E.); cameron.johnstone@strath.ac.uk (C.J.)

[3] El Colegio de la Frontera Sur, Department of Systematics and Aquatic Ecology, C.P 77014 Chetumal, Q. Roo, Mexico; mecallejas@ecosur.mx (M.C.-J.); malhaya@gmail.com (G.G.D.B.); lcarrillo@ecosur.mx (L.C.)

[4] School of Engineering, Cardiff University, Queen's Buildings, The Parade, Cardiff CF24 3AA, Wales, UK; AllmarkMJ1@cardiff.ac.uk (M.A.); Odoherty@cardiff.ac.uk (T.O.)

[5] Marine Resources Department, Center for Research and Advanced Studies of the National Polytechnic Institute, C.P. 97310 Mérida, Yucatán, Mexico; imarino@cinvestav.mx

[6] Instituto de Ingeniería, Universidad Nacional Autónoma de México, Cd. Universitaria, C.P. 04510 Mexico City, Mexico; RSilvaC@iingen.unam.mx

* Correspondence: s.ordonez@strath.ac.uk; Tel.: +44-(0)141-574-5019

check for updates

Abstract: Marine renewables represent a promising and innovative alternative source for satisfying the energy demands of growing populations while reducing the consumption of fossil fuels. Most technological advancements and energy yield assessments have focused on promoting the use of kinetic energy from tidal streams with flow velocities higher than $2.0 \, \mathrm{m\,s^{-1}}$. However, slower-moving flows from ocean currents are recently explored due to their nearly continuous and unidirectional seasonal flows. In this study, the potential of the Yucatan Current was analysed at nearshore sites over the insular shelf of Cozumel Island in the Mexican Caribbean. Field measurements were undertaken using a vessel-mounted Acoustic Doppler Current Profiler (ADCP) to analyse the spatial distribution of flow velocities, along with Conductivity-temperature-depth (CTD) profiles as well as data gathering of bathymetry and water elevations. Northward directed flow velocities were identified, with increasing velocities just before the end of the strait of the Cozumel Channel, where average velocities in the region of $0.88\text{–}1.04 \, \mathrm{m\,s^{-1}}$ were recorded. An estimation of power delivery using horizontal axis turbines was undertaken with Blade Element Momentum theory. It was estimated that nearly 3.2 MW could be supplied to Cozumel Island, amounting to about 10% of its electricity consumption.

Keywords: ocean current; kinetic energy; marine renewables; marine turbines; Cozumel Channel; Mexico

1. Introduction

The use of renewable energy baseload power is a growing concern to successfully reduce the dependency on fossil fuels and satisfy the increasing global energy demands [1]. Tides, ocean currents, thermal and/or seawater salinity gradients and waves are marine energy sources that could provide

up to 300 GW of global installed capacity by 2050 [2,3], which has led to innovative and promising technologies [4–6]. Ocean currents and tidal energy could represent an annual global potential of 800 and 300 TWh, respectively [7].

Despite the increased investment on marine energy technologies [8,9] and the deployment of the first two commercial arrays for tidal current approach [10,11], technological advancements are limited to specific regions, which decreases the global commercialisation of this technology. At the time of writing, tidal currents higher than 2.5 m s^{-1}, normally found in large shelf seas such as Western Europe, Yellow Sea and northern Australia, have been the focus of resource assessments and the implementation of large marine turbine systems [12]. If the viable threshold velocity required for the optimum operation of a turbine or converter decreases below 2.0 m s^{-1}, then the potential supply from ocean currents and tidal streams could increase dramatically, thus becoming a global commodity.

Ocean currents driven by wind stress, Coriolis force, pressure gradients, temperature and salinity gradients, friction and interactions with shorelines [13] could provide large advantages when compared to tidal currents as ocean currents show a nearly continuous and relatively constant unidirectional flow. Furthermore, ocean currents are globally extended and constitute an attractive alternative for marine renewables particularly at locations where flow acceleration is exacerbated as a consequence of the geomorphology and seabed topography such as straits and channels [2,8].

The energy potential of the ocean currents, such as in the Gulf Stream, has been recently assessed through the use of numerical models and flux observations [13,14]. Challenges related to the implementation of marine energy technology in the Gulf Stream are associated with difficulties arising with the installation of the devices in deep waters and long distances to shore [15,16]. However, there is still a lack of information related to energy yield assessments of open ocean currents around coastal areas.

The ocean current flowing along the Cozumel Channel in the Mexican Caribbean was investigated by the authors of [17,18]. Initial findings suggest that the flow speeds developed in the mid section of the Channel are in the order of 2.0 m s^{-1}. Nevertheless, these findings do not focus on shallow coastal waters (depths < 50 m), which could reduce excessive installation and maintenance costs associated with distances and water depths [15,16]. Thus, identifying physical and environmental constraints is required to assess suitable sites for the exploitation of the kinetic marine energy [19]. Unlike tidal streams, which can reach flow velocity magnitudes > 2 m s^{-1}, sometimes exceeding 5 m s^{-1} (e.g., [20]), ocean currents are slower, yielding less power but reducing the overall loading that marine turbines would need to withstand. In recent years, preliminary methodologies to design Horizontal Axis Tidal Turbines (HATTs) have been developed to maximise the hydrodynamic efficiency of a turbine operating at flow velocity magnitudes of 1.0–1.5 m s^{-1} [21].

Therefore, this study aimed to explore the potential of the nearby Yucatan Current in the western and northern insular shelf of Cozumel Island as a marine renewable energy source in the Mexican Caribbean. The analysis of the current over the shelf and its energy content were studied based on field measurements in order to: (i) provide a spatial characterisation of the flow (i.e., velocity magnitude and direction); (ii) recognise potential near-shore sites; and (iii) identify the physical features of the seabed (e.g., bathymetry) and environmental limitations (e.g., protected zones) in the area. Results were then used for an initial quantification of the power delivery that could be achieved with the use of HATTs and to assess the requirements of the technological development necessary for its implementation in the future.

2. Study Area

Located in the Mexican Caribbean, the Cozumel Channel is delimited by the eastern side of the Yucatan Peninsula and Cozumel Island (Figure 1). The Cozumel Channel is about 50 km long and 18 km wide with water depths reaching 500 m. It forms a passageway of ~5 Sv (5 Mm^3 s^{-1}) and 20% of the mean transport of the Yucatan Current [22] that flows northward parallel to the Yucatan Peninsula, eventually forming the Loop Current into the Gulf of Mexico and continuing as the Gulf Stream after

passing the Florida Channel [18,22,23]. The velocity magnitudes increase after crossing the Cozumel Channel reaching speeds of up to 2–2.5 m s^{-1} close to the Yucatan Channel [24] with average surface velocities of up to 1.5 m s^{-1} [23,25]. An average speed of 1.1 m s^{-1} was recorded across the Cozumel Channel, at 30 m of the water column in the central section of the strait [22]. The flow velocities within the Cozumel Channel are driven mainly by the ocean current, with limited influence of any other contributions (e.g., local wind, waves or tides). For instance, the tidal range in the Caribbean Sea is microtidal [26], with an average depth fluctuation of ∼0.18 m at Cozumel Island, based on seven-year records from pressure sensors [23].
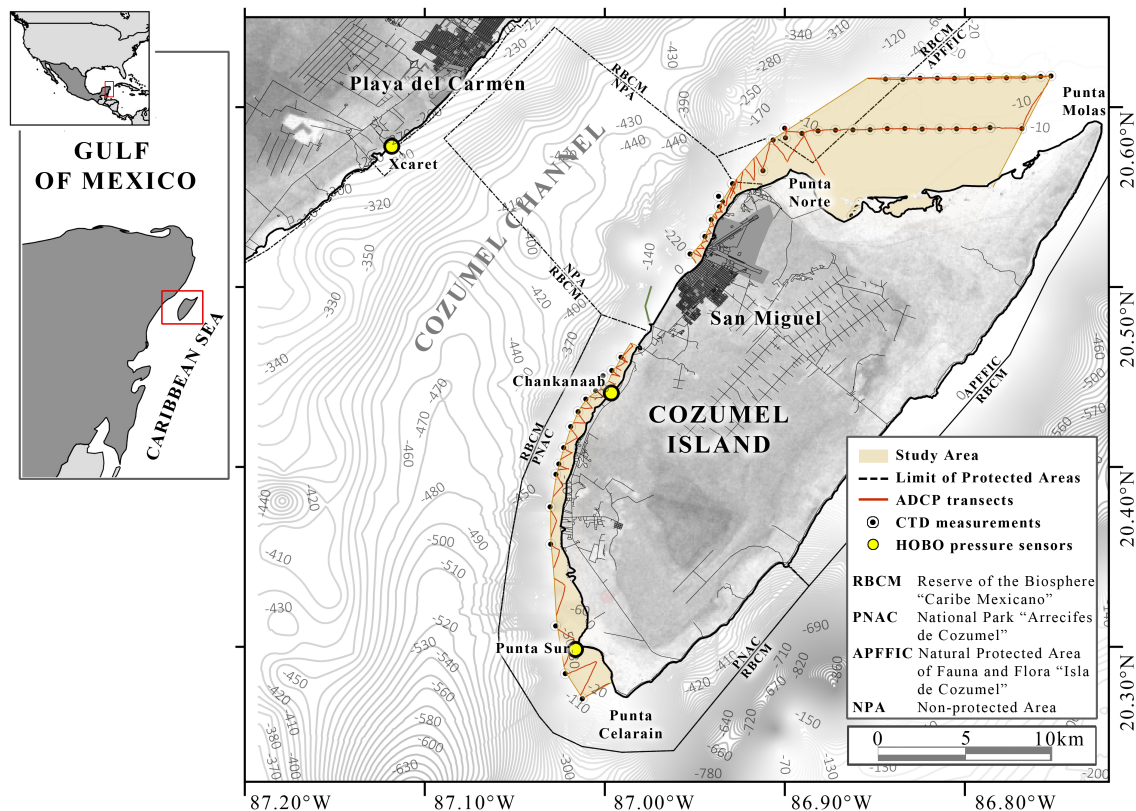
Figure 1. Map showing the location of the Cozumel Channel, marine protected areas, bathymetry and human settlements of Playa del Carmen and San Miguel (**right**). The locations of ADCP, CTD profile measurements along the study area as well as deployments of HOBO water level data loggers at Chankanaab (20.44111° N, 86.99639° W), Punta Sur (20.29853° N, 87.01632° W), and Xcaret (20.57826° N, 87.11834° W) are also shown.

The insular shelf of Cozumel Island features water depths up to 35–50 m and extends about 250–500 m from the shoreline (Figure 1). In the northern area, between Punta Norte and Punta Molas, the shelf extends for more than 15 km seaward, where sandy bottoms are found. The nearshore bathymetry comprises two shallow coastal terraces with coral reef lines followed by sandy plains before the steep insular shelf slope along the coastline from Punta Celarain to Punta Norte [27].

The annual electricity consumption in Cozumel Island was of ∼274.75 GWh in 2016 with a total expenditure of approximately US$ 30 million [28,29]. The growth in energy consumption relates to the accelerated growth rate of local population (San Miguel and Playa del Carmen), increasing from ∼7130 to ∼229,400 inhabitants during 1970–2010, as well as to cruising tourism arrivals with more than 4 million passengers per year with economic benefits of about US$ 762 million [30]. Cozumel Island is considered as the first cruising tourism destination worldwide [31], and for which the utilisation of marine renewables could contribute to afford a more sustainable energy supply, currently supported by a single submarine cable from mainland Mexico.

The coral reef systems alongshore the coastal waters of Cozumel Island represent the economic cornerstone in the region with several species mainly found in the east and south coast of the island [31]. For this purpose, three marine protected areas have been established [32–35] (Figure 1): (a) Reserve of the Biosphere "Caribe Mexicano" (RBCM); (b) National Park "Arrecifes de Cozumel" (PNAC) (11,988 ha) at the southwest coast of Cozumel Island; and (c) Natural Protected Area of Fauna and Flora "Isla de Cozumel" (APFFIC) at the north and northeast coast of Cozumel (37,829 ha). This information was utilised when assessing the establishment of an array of marine devices in the coastal areas of Cozumel.

3. Materials and Methods

3.1. Field Measurements

An overview of the ocean current circulation was made based on the HYbrid Coordinate Ocean Model (HYCOM) outputs, as presented in [36], for the coordinates 15.5–22.8° N and 85.5–89.0° W and a resolution of 1/12°. As a result, a map of the horizontal-surface velocity fields (i.e., magnitude and directionality) was obtained based on time-average of HYCOM daily data for the period 2010–2013 in the Mexican Caribbean and around Cozumel Island. HYCOM is a proved and validated model for several regions and represents fairly well the main oceanographic features in the study area as compared with observations (e.g., [18,37,38]).

Further analysis was conducted considering results from field measurements collected during 21–29 September 2018, over the western and northern insular shelf of Cozumel Island, where a feasible site of marine renewable conversion was identified from the Yucatan Current circulation. Water level variations were measured using HOBO® water level data loggers deployed at Xcaret, Chankanaab and Punta Sur (Figure 1), considering a sampling interval of 30 min to verify the microtidal conditions in the study area. Water level variations were referred to the average water level during the survey period, whereas the tidal range was estimated considering peak-to-peak variations.

The spatial variation of instantaneous flow velocities was measured throughout the west and north insular shelf of Cozumel Island. Flow velocity magnitudes and directionality were retrieved from Acoustic Doppler Current Profiler (ADCP) transects using a vessel-mounted RiverPro ADCP [39] equipped with a fully integrated GPS (Figure 1). The measurements were limited to water depths < 50 m before the sharp insular slope decays towards the centre of the channel (Figure 1). The spacing between transects was ∼2 km from Punta Sur to Chankanaab, and ∼0.5–1.0 km close to Punta Norte. Further transects were developed in the north of Cozumel Island with a total length of ∼8.0–13.0 km.

Rose diagrams of the ADCP data were obtained to define the distribution and direction of the flow over the insular shelf of Cozumel Island. As a result, a power per unit area (kW m^{-2}) map was developed considering the depth-averaged velocities from the ADCP transects. Flow velocity exceedance curves were also calculated for selected transects around more energetic locations. Bathymetric data were also recorded during the ADCP measurements and complemented with echosounder data from a GPS from Humminbird, model 899 CXI HD SI to provide larger detail currently not provided by available nautical charts (S.M. 922.400 and S.M. 922.500 from Secretaría de Marina [40]), as well as to access the viability of potential areas suitable to deploy marine turbines. Salinity and temperature profiles at water depths <50 m were measured at the end of each transect (Figure 1) using a CTD profiler from YSI CastAway to estimate water density and identify barotropic or baroclinic conditions within the study area.

3.2. Analytical Model

Initial estimates of the energy yield capabilities around Cozumel Island were obtained using the Blade Element Momentum (BEM) theory. This method is widely used in the wind and marine energy industries, as it is one of the simplest techniques to obtain accurate power outputs predictions of tidal/wind turbines. The BEM model utilised was coded at the University of Strathclyde and

implemented in Python 3. Optimisation algorithms were derived with the SciPy Optimize package (method of Sequential Least Squares Programming (SLSQP) to iteratively solve the induction factors within the simulations [41]. By using BEM theory, the performance of the rotor can be accurately predicted and the errors within the model are reduced, as the aerodynamic characteristics of each blade section complement the equations from momentum theory (lift, drag, chord length, and angle of attack).

A three-bladed horizontal axis tidal stream turbine specially designed to operate in lesser energetic flows [21] was employed in this study. To account for inherent limitations of the analytical model, Prandtl tip and hub correction factors were included in each iteration [42]. The Buhl high induction correct factor was also utilised to account for axial induction factors greater than the theoretical limit [43]. The lift and drag coefficients of the aerofoil, developed by the National Advisory Committee for Aeronautics (NACA), in each section of the NACA 63-8xx blade were obtained from Encarnacion and Johnstone [21], based on ANSYS Fluent results for angles of attack of $-20°$ to $16°$. The Viterna-Corrigan post-stall model [44] was also used to evaluate the aerodynamic characteristics of the section upon the onset of stall operation ($\alpha = 16°$).

Four selected ADCP transects were used in the simulations based on their energy content and environmental constraints of the site. Within each transect, three 10 m windows separated by at least 50 m, centre-to-centre, and located over a relatively flat seabed profile (i.e., <1 m depth difference within 10 m along the seabed), were evaluated to obtain an averaged velocity profile. The obtained averaged profiles were then fitted to a power law function (Equation (1)), where the average value of the variables $\overline{U}_o$, flow velocity, and b ,the power law exponent, were used as inputs for the BEM simulations. It was decided to filter values of b that reached a power law relationship of 1×10^7 (i.e., a nearly constant velocity profile) so that at least 60% of the profiles obtained in any 10-m window resulted in values of $b < 10$.

$$U_o(z) = \overline{U}_o\, z^{1/b} \tag{1}$$

Two cases were evaluated for each window considering different turbine positions within the water column (Figure 2): (i) at the middle of the water column; and (ii) closer to the upper surface, establishing a 2.5 m clearance from the mean water surface and the blade tip positioned at the top dead centre. Therefore, the power output and corresponding C_P values (power coefficients) could be obtained for each case.
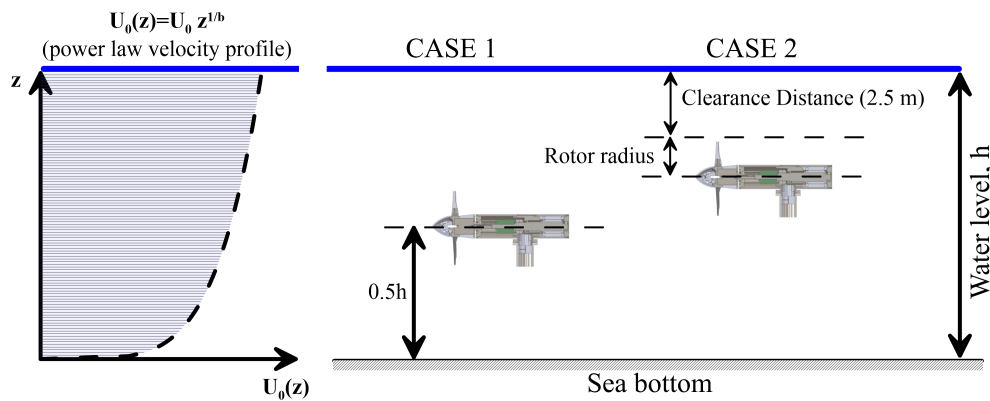
Figure 2. Case studies for BEM simulations considering the hub location within the water column as well as the development of velocity profiles based on power law fitting curve based on ADCP measurements

The performance of the rotor operating at peak power was considered in the simulations. Previous analysis by Encarnacion and Johnstone [21] showed that this operating point occurs at tip speed ratio (TSR) of 6.75. The diameter of the rotor was limited to 5 m since large diameter rotors will require complex gearing mechanisms, thus increasing the cost of turbines.
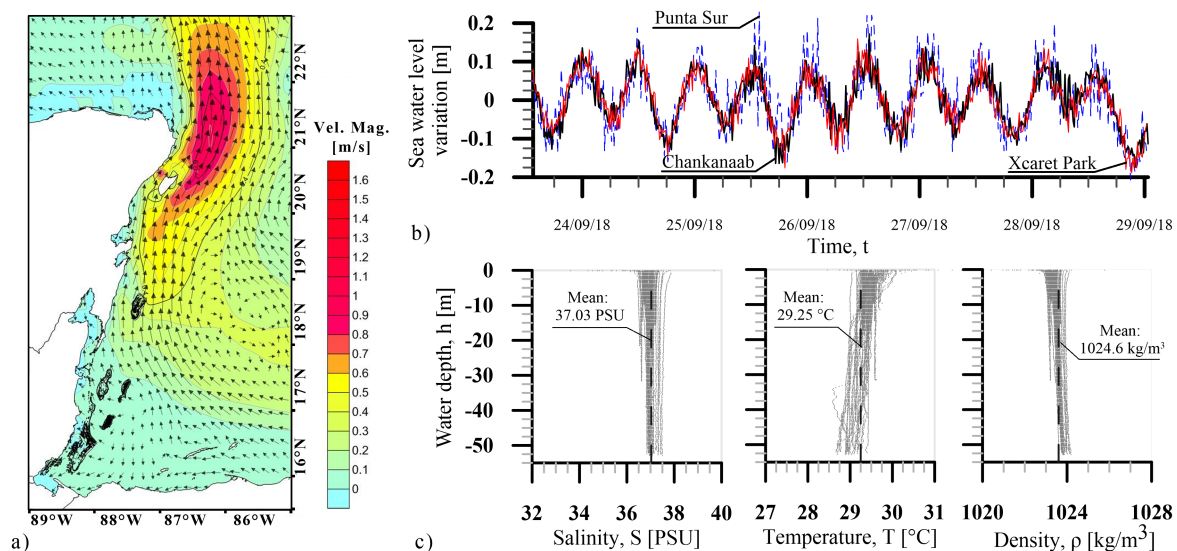
4. Results

4.1. Flow Velocities and Power Estimation

A preliminary description of the circulation related to the eastern Yucatan coast and its relationship with the Cozumel Channel resulted in the velocity field averaged over 2010–2013, as shown in Figure 3a and presented by Martínez et al. [36]. As can be seen in Figure 3a, the current is predominately flowing in a northerly direction from a latitude $\sim$19.5° N and beyond $\sim$22° N. It flows almost parallel to mainland Mexico with average velocity magnitudes increasing northwards, where flow velocities higher than 1.0 m s^{-1} were obtained. In the southern region, velocity magnitudes of $\sim$0.2–0.4 m s^{-1} can be observed at latitudes below 20° N, before the Cozumel Channel divides the Yucatan Current. The flow velocities within the Cozumel Channel increase rapidly, reaching values higher than 1.0 m s^{-1} at a latitude of 20.5–20.6° N (Figure 3a). The effect of Cozumel Island over the Yucatan Current is also evident when observing the increase of flow velocities at the east of the Island.

Measured sea water level variations from pressure sensors (HOBO Water level loggers) provided a seven-day averaged water level or peak to peak range of 0.23 m and 0.24 m ($\sigma = \pm 0.04$ m) for the Xacret and Chankanaab regions, respectively (see Figure 3b). An increase in the water level range during the field survey period was observed in Punta Sur with an average amplitude of 0.31 m and $\sigma = \pm 0.04$ m. Maximum amplitude range occurred at Punta Sur with 0.38 m, whereas the minimum was reached for Xcaret with 0.16 m (i.e., similar to Chankanaab). The microtidal regime within the Cozumel Channel thus features semidiurnal behaviour with a water level range of 0.26 m ($\sigma = \pm 0.04$ m) (Figure 3b). Although seawater level fluctuations occur in the study area, the main forcing for the development of kinetic energy within the Channel is noticeably driven by the ocean current rather than tidal like oscillations.

Temperature and salinity profiles resulting from CTD measurements were shown to be nearly homogeneous throughout the water column for the entirety of the field survey, thus indicating barotropic conditions for the west shallow waters of the Cozumel Channel (Figure 3c). Average values of salinity and temperature were of 37.03 PSU ($\sigma = \pm 0.05$ PSU), and 29.25 °C ($\sigma = \pm 0.05$ °C) leading to a water density of 1023.6 kg m^{-3}.

Figure 3. Flow velocity magnitudes and circulation of the Yucatan Current in the Caribbean Sea (**a**). Results of sea water level variations in Chankanaab, Punta Sur and Xcaret (**b**), from field measurements within the Channel as well as temperature, salinity and water density (**c**) during the field survey period (23–29 September 2018).

Flow velocity direction and magnitudes along the insular shelf of Cozumel are further described in detail based on ADCP in-situ measurements. The general rose diagram in Figure 4 (left) demonstrates that the flow direction oscillates between $30° < \theta < 90°$, but it is predominantly driven towards the northeast (40–50°), aligned with the ocean current flow. Rose diagrams for different regions (Z1–Z4) are portrayed in Figure 4 (right). The highest velocity magnitudes of about 0.6–1.2 m s^{-1} (relative frequency >72%) occurred in the northern region of the Channel, between latitudes 20.53° N and 20.57° N (Figure 4b, Zone Z2). For latitudes > 20.57° N (Figure 4a, Zone Z1), over the insular shelf and between Punta Norte and Punta Molas, flow velocity magnitudes decrease considerably (i.e., about 82% with velocity magnitudes 0–0.3 m s^{-1}), possibly caused due to the Cozumel Channel widening.

Between latitudes 20.53°N and 20.44°N (Figure 4c, Zone Z3), the rose diagram exhibits components oriented NNE and SSW. A counter-current flow of <0.4 m s^{-1} was measured with directions between $230° < \theta < 270°$ (i.e., SSW and S) and appears to be particularly limited to this zone. At latitudes <20.44° N (Figure 4d, Zone Z4), the velocity magnitude is mainly directed towards the north with almost 90% of the flow velocity magnitudes <0.6 m s^{-1}.
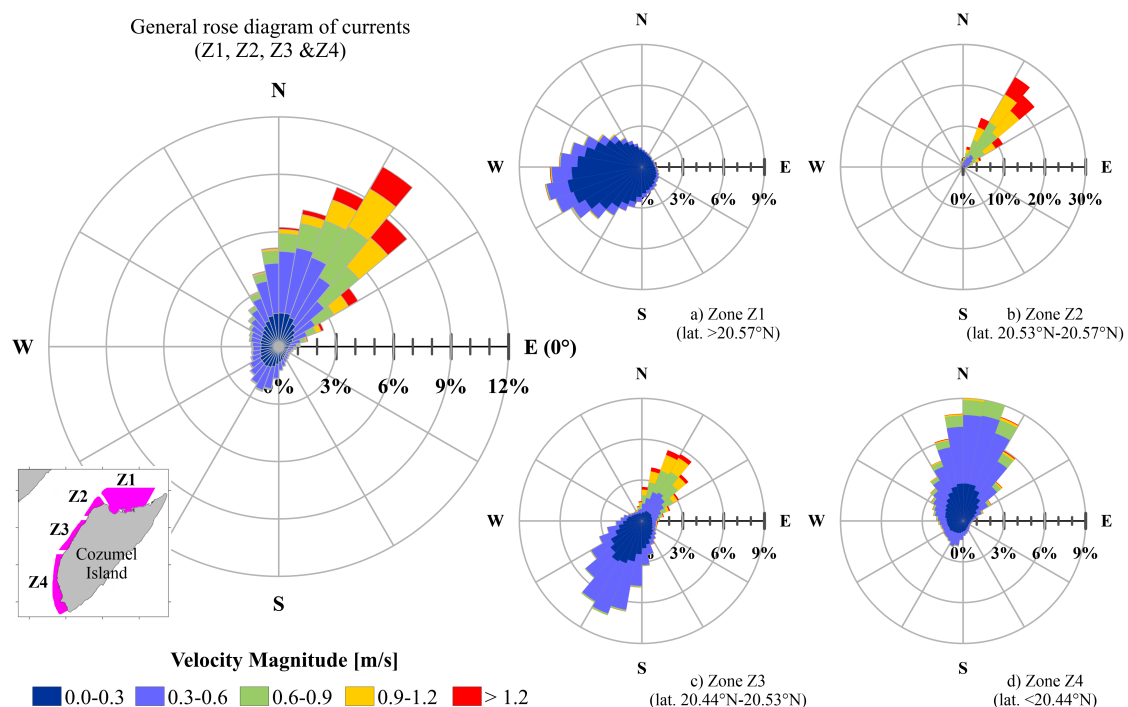
Figure 4. General rose diagram of currents along the east and north shallow waters of the Cozumel Channel (**left**), and for Zones Z1–Z4 featured by different conditions of flow direction and velocity magnitude (**right**).

In Figure 5a, the distribution of power per unit area is described for the east shallow coastal waters of the Cozumel Channel. The power per unit area was calculated as P/A = $0.5\rho\overline{V_{Mag}}^3$ given in W m^{-2}, with $\overline{V_{Mag}}$ as the depth-averaged velocity magnitudes from ADCP measurements and ρ as the average water density resultant from CTD results (1023.6 kg m^{-3}). Most values of power per unit area were in the order of 0–10 W m^{-2}, with some areas of 10–70 W m^{-2} (e.g., Chankanaab). Values larger than 500 W m^{-2}, reaching up to 2500 W m^{-2}, occur within a narrow strip of ∼200–250 m width, mainly in Zone Z2 (Figure 5b) and close to the steep slope of the insular shelf (Figure 5c). These values are located within a non-protected area (NPA), south of the limit with the Natural Protected Area of Fauna and Flora "Isla de Cozumel" (APFFIC) and close to the northern portion of the city of San Miguel (Figure 5).
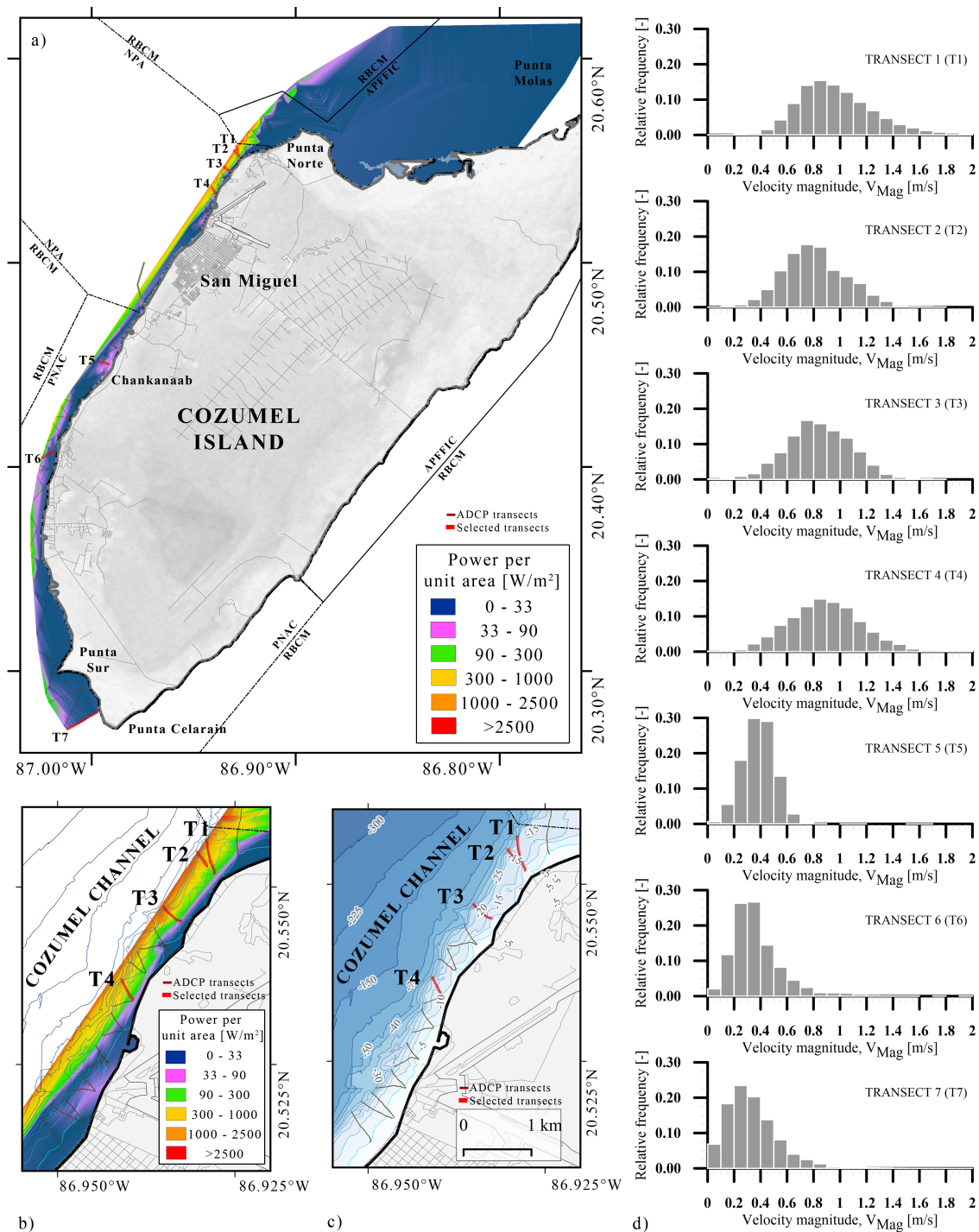
Figure 5. Power per unit area based on ADCP in-situ measurements for: (**a**) the shallow east coastal waters of the Cozumel Channel; and (**b**) Zone Z2 (latitudes ∼20.53° N–20.57° N). Bathymetric details in Zone Z2 are shown in (**c**) for the selected Transects T1–T4. Histograms are shown in (**d**) for different Transects T1–T7 along the west coast of Cozumel Island.

Histograms of velocity magnitude from ADCP measurements at different transects distributed along the west side of the Cozumel Island are shown in Figure 5d. Velocity magnitudes varied from 0.34 m s^{-1} to 1.04 m s^{-1} (Table 1), with average among transects of 0.71 m s^{-1} ($\sigma = \pm 0.23$). The lower velocities were observed closer to the coastline, and the higher velocities occur close to the limit edge of the insular shelf (Figure 5).

Table 1. Velocity magnitude, flow direction and coordinates of selected transects in the east-coast of Cozumel Channel.

| Transect		Latitude (°)	Longitude (°)	Length (m)	Depth-Averaged Vel. $\overline{V_{Mag}}$ (m s^{-1})	Depth-Averaged Vel. Fluct. (σ) (m s^{-1})	Direction* (θ) (°)	Direction Fluct. (σ) (°)
T1	Start	20.5524	−86.9279					
	End	20.5567	−86.9290	489.5	0.98	0.30	50.00	14.49
T2	Start	20.5529	−86.9288					
	End	20.5549	−86.9302	250.0	1.03	0.24	48.60	13.05
T3	Start	20.5452	−86.9326					
	End	20.5472	−86.9351	340.8	1.04	0.24	48.34	13.13
T4	Start	20.5138	−86.9496					
	End	20.5179	−86.9524	317.8	0.83	0.30	62.74	24.25
T5	Start	20.4515	−86.9962					
	End	20.4504	−86.9919	470.6	0.39	0.12	267.23	33.80
T6	Start	20.4041	−87.0246					
	End	20.4076	−87.0187	722.4	0.37	0.19	70.03	31.96
T7	Start	20.2797	−86.9974					
	End	20.2714	−87.0119	1778.7	0.34	0.20	73.09	43.94
Average				624.3	0.71	0.23	88.58	24.95

* The velocity direction is referred to the east and positive anticlockwise.

The velocity magnitude distributions recorded were found to gradually shift when moving from southern to more northern transects (Figure 5d). Zone Z2, represented by Transects T1–T4, shows the highest velocity magnitudes with an average of 0.93 m s^{-1} ($\sigma = \pm 0.30$) and 81.9–93.4% of the velocity distribution with values higher than 0.6 m s^{-1}. Peak velocities magnitudes of ∼1.8–1.9 m s^{-1} were identified in Transects T1–T4, which represent an increase rate of 0.05–0.06 m s^{-1} per kilometre. This could occur due to the effect of the main current flow moving closer from the centre of the Cozumel Channel to the shoreline in the northern zone (Z2). In this area, the velocities and power per unit area (Figure 5b,d) seemed to escalate just before the stretching end of the Cozumel Channel and the broadening of the insular shelf, which is more prone to effect the main flow passing through. For Transects T5–T7 (Zones Z3 and Z4), the average velocity magnitude was observed to be as low as 0.3–0.4 m s^{-1} (i.e., half the velocities at transects in Z2), with about ∼89.3–97.2% of the velocity distribution below 0.6 m s^{-1}.

The average flow direction considering T1–T7 was of ∼88.6° ($\sigma = \pm 25.0$ °) and seemed to be affected by the coastline orientation (i.e., gradually modified from 73.69° in the south to 50° in the northern area). Around T5, the effect of a counter-current of ∼0.38 m s^{-1} was identified (Figure 4c and Table 1), which could be caused by the interaction of the northward flowing current with the insular geomorphology. For Transects T1–T4, the average flow direction was of ∼51.6° ($\sigma = \pm 17.0$ °) (NNE), with larger flow direction variability observed for T1 and T4, but reduced for T2 and T3 (Table 1). This flow directionality results in similarities observed in UK tidal sites with variations of 20° [45].

Exceedance curves of flow velocity magnitudes as well as flow velocity profiles were developed for Transects T1–T4 in the northern area (Table 1 and Figure 6a), where the highest power per unit area and velocity magnitudes were found (Figure 5). For these transects, the velocity magnitudes $V_{Mag} > 1.6$ m s^{-1} have a probability of exceedance f < 1.0%. These high-intensity flow speeds reach a maximum of 2.7 m s^{-1}. For a probability exceedance f = 10.0%, the velocity magnitude was of $V_{Mag,T1} \approx 1.41$ m s^{-1}, $V_{Mag,T2} \approx 1.34$ m s^{-1}, $V_{Mag,T3} \approx 1.18$ m s^{-1} and $V_{Mag,T4} \approx 1.20$ m s^{-1}. Moreover, for a probability of exceedance f = 90%, important velocity magnitudes were found for T2–T4: $V_{Mag,T2} \approx 0.74$ m s^{-1}, $V_{Mag\,T3} \approx 0.44$ m s^{-1} and $V_{Mag,T4} \approx 0.47$ m s^{-1}. The lower values obtained for T1 and f = 90% $V_{Mag,T1} \approx 0.26$ m s^{-1} represent a larger variability of the flow velocities possibly caused by the lower velocities close to the shoreline, as shown in Figure 6b. Particularly for T2, the velocities are quite uniform at 20 m water depth at a distance of ∼150 m from the shoreline. A submarine mound is later found, where the insular shelf edge is located (Figure 6b) and where velocity magnitudes close

to 1.2 m s^{-1} were measured. T3 and T4 present similar patterns as those observed on the exceedance curves in Figure 6a, with comparable values of f = 10%, 50% and 90%.
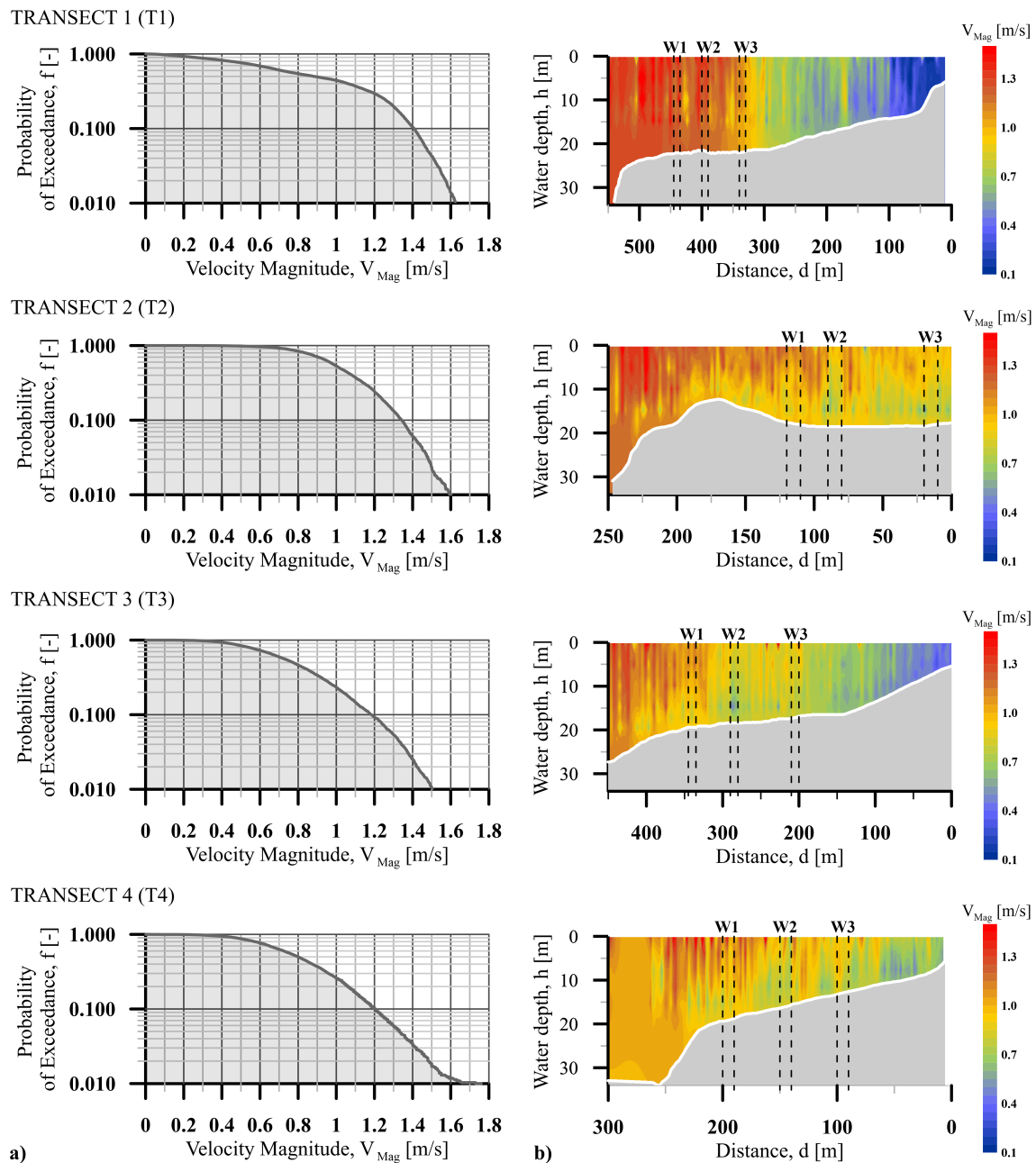
Figure 6. Transects T1–T4 in the north-west portion of Cozumel Island: (**a**) exceedance curves of marine current velocities; and (**b**) velocity profiles. Location of 10-m windows (W1–W3) at each transect for a practical estimate of the power output.

The flow velocity presents a relevant variation along the profiles for the selected transects (Figure 6b). In this regard, velocity magnitudes larger than 1.0 m s^{-1} were mostly found at 150 m shoreward from the insular slope, almost uniform with the water depth, up to ~20 m. Velocities were observed to decrease significantly with values of about 0.2–0.4 m s^{-1} close to the shoreline, which is expected to occur due to bottom friction and the shallower water depth as observed in T1, T3 and T4 (Figure 6b). Effects of bottom friction could be noticed within a layer of about 7 m from the sea bottom, mainly shown in T2–T4 and on a smaller portion in T1.

Bottom profiles given in Figure 6b also represent typical profiles along the west coast of Cozumel Island. T1 and T2 show the development of the insular shelf slope, which was observed to start at water depths of ∼35 m. Transect T4 presents a slope of 1:10, which further develops on a steep slope (1:5) at ∼20–34 m depth and a terrace of 50 m before reaching the end of the insular shelf. Transects T1 and T3 developed a slope before a terrace at 20 m depth is noticed. From the records obtained in the field survey, the extent of the insular shelf was estimated to be within 250–500 m (Figure 5c). It is worth noting that the flow velocity magnitude (∼0.4–1.4 m s^{-1}), as well as bathymetric variations observed in Transects T1–T4 (Figure 6b), represent important design decision parameters that need to be considered in the implementation of marine turbines in nearshore sites of the Cozumel Channel.

4.2. Power Output

The location of three 10 m windows was established for each of Transects T1–T4. The velocity distribution profiles served as an input to calculate the power output of a 5 m diameter HATT installed over the insular shelf of the Cozumel Channel. The average value of the variables $\overline{U}_o$ and b obtained as inputs to the BEM simulations are described in Table 2. It should be noted that b-values for each transect varied from 2.5 to 6.5, indicating greater bed roughness than the usual 1/7th power law applied to more theoretical estimations, which could be induced by the reef systems.

Table 2. Average values of $\overline{U}_o$, b, water depth and distance from the shelf edge for each 10-m window.

Transect ID	Window	$\overline{U}_o$ (m/s)	b	Water Depth (m)	Distance * (m)
T1	1	0.85	4.99	19.43	105–115
	2	0.85	3.08	18.52	150–160
	3	0.80	5.43	17.88	210–220
T2	1	1.13	3.11	17.83	130–1405
	2	1.12	2.82	18.47	160–170
	3	1.16	3.05	18.15	230–240
T3	1	0.86	4.99	19.43	105–115
	2	0.79	6.89	18.47	160–170
	3	0.81	2.60	17.62	240–250
T4	1	0.88	6.14	19.06	100–110
	2	0.74	6.26	16.07	150–160
	3	0.87	4.32	12.86	200–210

* Distance measured shoreward with the shelf edge considered as zero reference.

The resultant power outputs obtained from the analytical model and the velocity power law profiles are shown in Table 3. The power outputs were 7.8% greater for the "floating turbine" (Case 2) than for the "bottom mounted" device (Case 1) (Figure 2).

The power output in T2 by three turbines can reach values in the scale of 8.87 kW and 13.39 kW for Cases 1 and 2, respectively (Table 3). This result was expected as the value of $\overline{U}_o$ for T2 was higher than for all other transects. The lowest C_P for this transect was observed in the second window and attributed to the low value of b. The lower is the value of b (Table 2), the quicker do the flow velocity magnitudes decay to zero values towards the bottom, resulting in lower average flow speed over the rotor in addition to higher load variability resulting in fatigue damage.

The centre-to-centre distance of each window within one transect was initially defined on 50 m. However, since the flow velocity was noticed to be mainly perpendicular to the transect, a large number of turbines may be placed between windows to maximise the power output of each transect. This array formation implies that the flow on each turbine is not reduced, as they are considered to be installed on a staggered array downstream.

The power output for each window in a transect does not show significant variations (Table 3), except for T4 where a steeper seabed profile occurs reaching a water depth of 12.86 m in the last

window (Table 2). Thus, the estimate of the power output for each transect (relative to the number of turbines) was obtained as the average power output of the initial set of three turbines multiplied by a factor n = 1, 2, 3; where n = 2 translates to six turbines and n = 3 translates to nine turbines, n denoting the number of turbines per window. Table 4 shows the expected power output for each transect given this estimation.

Table 3. Power output (P), power coefficients (C_P) and total theoretical power derived from BEM for each of the 10-m windows within the selected Transects T1–T4.

Transect ID		Window 1	Window 2	Window 3	Total Power (kW)
		Case 1—Bottom Mounted			
T1	Power (kW)	1.69	1.29	1.46	**4.43**
	C_P	0.27	0.21	0.28	
T2	Power (kW)	3.19	2.68	3.01	**8.87**
	C_P	0.20	0.19	0.21	
T3	Power (kW)	1.75	1.50	1.02	**4.27**
	C_P	0.27	0.31	0.19	
T4	Power (kW)	2.02	1.21	1.70	**4.93**
	C_P	0.30	0.30	0.25	
		Case 2—Floating Device			
T1	Power (kW)	2.17	1.92	1.80	**5.89**
	C_P	0.35	0.31	0.35	
T2	Power (kW)	4.75	4.17	4.42	**13.34**
	C_P	0.30	0.30	0.30	
T3	Power (kW)	2.24	1.78	1.53	**5.56**
	C_P	0.35	0.37	0.28	
T4	Power (kW)	2.45	1.42	1.98	**5.86**
	C_P	0.36	0.35	0.30	

Table 4. Power output for Transects T1–T4 relative to the number of turbines placed for each case condition.

Number of Turbines	3 (n = 1)	6 (n = 2)	9 (n = 3)	12 (n = 4)	15 (n = 5)
Centre to Centre Distance *	50.0 (10D)	20.0 (4D)	12.5 (2.5D)	9.1 (1.8D)	7.1 (1.4D)
Transect ID	**Case 1—Bottom Mounted**				
T1	4.43	8.87	13.30	17.74	22.17
T2	8.87	17.75	26.62	35.49	44.36
T3	4.27	8.53	12.80	17.07	21.34
T4	4.93	9.87	14.80	19.73	24.66
Total Power Output (kW)	**22.5**	**45.02**	**67.52**	**90.03**	**112.53**
Transect ID	**Case 2—Floating device**				
T1	5.89	11.79	17.68	23.57	29.47
T2	13.34	26.68	40.02	53.36	66.70
T3	5.56	11.12	16.67	22.23	27.79
T4	5.86	11.72	17.58	23.44	29.30
Total Power Output (kW)	**30.65**	**61.31**	**91.95**	**122.6**	**153.26**

* The centre to centre distance is also referred as a function of the turbine diameter (D).

Increasing the number of turbines deployed within the studied sections results in substantial power outputs in the order of 153 kW. While this seems favourable, it decreases the spacing between each turbine. Sutherland et al. [46] undertook a study considering cross-flow turbines, and found that a spacing of 3D decreases the power output of such devices. Although the devices analysed were axial flow turbines, the decreased spacing (2.5D and lower) might result in flow interaction and performance losses. Regardless, the use of a 2.5D lateral spacing between turbines could potentially signify an average hydrodynamic power output closer to 23 kW per row (according to Table 4, Case 2 and a nine-turbine array).

Assuming a lateral spacing of 2.5D [46] and a downstream spacing of 10D (50 m), according to the available literature [47]; an array of "floating turbines" (Case 2) could be potentially installed along ∼5 km in the northern region Z2, from San Miguel to the limit with the APFFIC (Figure 1). This region is characterised by flat seabed areas that extend 100 and 200 m from from the insular shelf edge, along 0–3 and 3–5 km northward San Miguel, respectively. This region is located outside environmental protected areas and might not interfere with tourism activities and navigational channels, thus providing an ideal location for the deployment of the turbine array. Therefore, nearly 3.2 MW could be produced using three bladed horizontal axis devices, which represents 10% of the energy demands of Cozumel Island.

Further estimations will need to consider the temporal variability of the current around region Z2, which at this stage has been considered as a current of continuous nature. The use of other technologies, such as vertical axis, cross flow or kite mounted turbines should also be considered where floating HATTs cannot be deployed.

5. Discussion and Concluding Remarks

The kinetic energy of the Yucatan Current flowing over the insular shelf of Cozumel Island was spatially analysed. A review of the averaged flow velocity from daily HYCOM outputs as presented in [36] showed that the energy potential around Cozumel Island could reach flow speeds higher than 1.2 m s^{-1} in some regions. The microtidal conditions for the study area (water level range of 0.26 m, $\sigma = \pm 0.04$ m) also provided additional evidence that the current flow is mainly driven by a nearly continuous and almost constant ocean current, contrary to tidal streams that vary in both directionality and intensity [48,49]. However, further research is required to estimate the contribution of the average microtidal signal to the ocean current velocities, and consider field validation along the Mexican Caribbean as well as detailed modelling within the Cozumel Channel and its coastal areas. In addition, a tidal analysis should be performed to determine the sea water level fluctuations for the study area considering longer time series of sea level records than those contemplated at present in order to provide a more accurate prediction.

In the south region of Cozumel Island (Zone Z3 and Z4), flow velocity magnitudes below 0.6 m s^{-1} are mostly developed, matching to locations where coral reef formations and tourism activities are largely featured as the cornerstone of the economic activities in the study area (i.e., scuba diving, snorkelling and aquatic sports) [31], making it an unsuitable location to deploy marine energy converters. In the central area (Zone Z3), a counter-current with velocity magnitudes of ∼0.4 m s^{-1} was identified, as also observed in previous studies [23,50]. This flow pattern could relate to the interaction of the current with the coastline morphology and where infrastructure is mainly developed (i.e., cruise ship piers and sea terminals). The energy potential in Z3 is further constrained by the water depth, bathymetric changes (e.g., steep slopes), bottom friction (e.g., induced by large roughness from reef systems), coastline shapes and orientation, as well as possible interaction with maritime infrastructure.

The most suitable areas to harvest energy from the ocean current by marine turbines are found in Zone Z2, closer to the northern insular shelf-edge of Cozumel Island with an energy content of nearly 0.5–2.5 m^{-2}. An average velocity of 0.93 m s^{-1} ($\sigma = 0.30$ m s^{-1}) and peak flow velocities in the range of 1.8–1.9 m s^{-1} were detected at water depths between 20 and 35 m, which are suitable for the installation of floating devices. A specific area located between latitudes 20.5185 to 20.5524° N and outside the delimitation framed by marine protected areas, navigational channels and tourism activities was of

particular interest. It extends to approximately 5 km long and 100–200 m wide corresponding to circa 70 ha of the seabed. All these characteristics indicate that this particular region within Z2 should be considered as the prime location to deploy marine energy devices in the insular shelf of the Cozumel, which also benefits from sandy bottoms with low presence of coral reef formations [51–53], thus decreasing possible damage to the ecosystem.

Challenges associated with the design of marine energy converters should consider additional parameters related to the flow characteristics. The averaged flow direction in Zone Z2 was predominantly NE ($\sim$51.6° and σ = $\pm$17.0°), aligned with the ocean current flow and similar to that observed on tidal streams [45]. Nevertheless, power losses could be expected as a consequence of the directional fluctuations. Considering results for all transects over the east coast of the Cozumel Channel, local fluctuations on flow directionality were observed to be mainly developed due to the coastline orientation. As this study was primarily based on spatial variability measurements, temporal variations of the flow in this region must be carried out in the future to account for further flow particularities that are time-variable and time-dependent and relevant to turbine designing; e.g., turbulence length scales, turbulent kinetic energy, wave-current interactions, etc., which may be more detrimental in slower flow streams [54].

Given the flow intensities and the locations prone to harvest energy from the oceanic current, HATTs were considered as the most feasible option as this may lower the costs by minimising learning procedures established by those that are already in use. Additionally, higher power efficiencies have been reported with their use compared with other technologies; for example, the device used in [46]. The present study has shown the possibility of utilising floating turbines in the order of 5 m in diameter, able to achieve a maximum C_P of $\sim$0.35 at a TSR = 6.75. As expected, the closer the turbine is to the surface, the more energy can be captured, which translates to an average improvement of 7.80% when compared to the bottom mounted device. These floating devices of 5 m of rotor diameter may become more cost effective with time since operational procedures can be minimised due to their accessibility [55]. Further investigations will consider relations between rotor diameter and cost of energy.

It was foreseen that nearly 3.2 MW could be supplied (i.e., 10% of the electricity consumption), considering an array of devices along 5 km in Zone Z2 with a lateral and downstream spacing of 2.5D and 10D, respectively. It is clear that the dynamics of the fluid will change drastically with the deployment of turbine arrays; therefore, the assumptions used to calculate the energy yield of a farm may not be completely realistic [56]. Despite the conjectures employed for the latter part of this analysis, the lateral and downstream spacing applied in this study were retrieved from existing physical and numerical modelling of tidal turbine arrays giving an insight into the energy delivery that can be achieved with the proposed technology in this small section of the Channel. Clearly, the investigation of turbine interactions is an ongoing research question, and it is anticipated that the power output and loading characteristics of individual turbines within an array will be site dependent.

This estimate may be somewhat discouraging, however the implementation of devices in sites influenced by strong ocean currents compared to tidal energy sites provides advantages such as: (a) the continuous and almost uniform energy generation due to the single-directional current flows (i.e., not dependent on the tidal cycle); and (b) the possibility of reducing operational and maintenance costs using lightweight and inexpensive materials that could also benefit the development of turbine arrays in the region but this will be contemplated in future work. Moreover, it should be noted that the region evaluated in this study is only a small proportion of the channel, which corresponds to less than 1% of the channel's width. According to the convention reported in [56], the array proposed here can be identified as a medium size marine farm. Additional work will not only contemplate a better estimate of the overall power output based on numerical evaluations done explicitly for this region but also extend this analysis to other potential sites, for example the mainland side of the Cozumel Channel (i.e., closer to Playa del Carmen), where large tourism developments can be found.

It is noteworthy that technology available is currently not fully developed to be used in sites such as those found along the Cozumel Island. Concerns must be addressed to engineer an efficient device for turbine operation under these conditions. One of the main limitations could be related to the aspect ratio of the rotor blades [21]. A turbine design able to operate at high rotational speeds due to the velocity flow ($\sim$1.0 m s^{-1}) will inherently need to employ slenderer blades than those used to date, which could lead to rapid failure considering the shear and turbulent flows of the current [57,58], hence the importance of temporal flow studies in Z2.

The implementation of marine energy innovative technologies, such as HATTs or further, may tackle to some extent the electric demands of Cozumel Island, which increase rapidly mainly due to tourism activities. The transition to a renewable energy baseload system should also consider hybrid renewable energies solutions [59]. Hybrid systems could reduce the levelised costs of energy in Cozumel, according to studies done by the authors of [60,61]. Future work should consider the cost of energy associated with the implementation of a marine turbine array in the insular shelf of Cozumel, including capital and operational costs to envisage the techno-economic opportunities that could be achieved with the implementation of marine renewables in the area.

Conflicts of Interest: The authors declare no conflict of interest. The founding sponsors had no role in the design of the study; in the collection, analyses, or interpretation of data; in the writing of the manuscript, and in the decision to publish the results.

References

1. Jenniches, S. Assessing the regional economic impacts of renewable energy sources—A literature review. *Renew. Sustain. Energy Rev.* **2018**, *93*, 35–51. [CrossRef]
2. Huckerby, J.; Jeffrey, H.; de Andres, A.; Finaly, L. *An International Vision for Ocean Energy. Version III*, 2nd ed.; Ocean Energy Systems Technology Collaboration Programme: Lisbon, Portugal, 2016. Available online: www.ocean-energy-systems.org (accessed on 13 October 2018).
3. Jeffrey, H.; Jay, B.; Winskel, M. Accelerating the development of marine energy: Exploring the prospects, benefits and challenges. *Technol. Forecast. Soc. Chang.* **2013**, *80*, 1306–1316. [CrossRef]
4. Khan, N.; Kalair, A.; Abas, N.; Haider, A. Review of ocean tidal, wave and thermal energy technologies. *Renew. Sustain. Energy Rev.* **2017**, *72*, 590–604. [CrossRef]
5. Matthew, G.J.; Fitch-Roy, O.; Connor, P.; Woodman, B. *ICE Report T2. 1.1-Smart Peripheral Territories Transitions: Literature Review and Current Status*; Technical Report; University of Exeter: Exeter, UK, 2018.
6. Uihlein, A.; Magagna, D. Wave and tidal current energy—A review of the current state of research beyond technology. *Renew. Sustain. Energy Rev.* **2016**, *58*, 1070–1081. [CrossRef]
7. Bhuyan, G.S. Harnessing the power of the oceans. *IEA OPEN Energy Technol. Bull.* **2008**, *7*, 30–35.
8. Kerr, D. Marine energy. *Philos. Trans. R. Soc. A Math. Phys. Eng. Sci.* **2007**, *365*, 971–992. [CrossRef]
9. Pelc, R.; Fujita, R.M. Renewable energy from the ocean. *Mar. Policy* **2002**, *26*, 471–479. [CrossRef]
10. Nova Innovation Ltd. Nova M100-D. Available online: https://www.novainnovation.com/nova-m100-d (accessed on 13 March 2019).
11. Simec Atlantis Energy. Meygen. Available online: https://simecatlantis.com/ (accessed on 13 March 2019).

12. Zhou, Z.; Benbouzid, M.; Frédéric Charpentier, J.; Sciiller, F.; Tang, T. A review of energy storage technologies for marine current energy systems. *Renew. Sustain. Energy Rev.* **2013**, *18*, 390–400. [CrossRef]

13. Yang, X.; Haas, K.A.; Fritz, H.M. Theoretical Assessment of Ocean Current Energy Potential for the Gulf Stream System. *Mar. Technol. Soc. J.* **2013**, *47*, 101–112. [CrossRef]

14. Haas, K.; Yang, X.; Neary, V.; Gunawan, B. Ocean Current Energy Resource Assessment for the Gulf Stream System: The Florida Current. In *Marine Renewable Energy*; Springer International Publishing: Cham, Switzerland, 2017; pp. 217–236.

15. Hanson, H.P. Gulf Stream energy resources: North Atlantic flow volume increases create more power. *Ocean Eng.* **2014**, *87*, 78–83. [CrossRef]

16. Yang, X.; Haas, K.A.; Fritz, H.M. Evaluating the potential for energy extraction from turbines in the gulf stream system. *Renew. Energy* **2014**, *72*, 12–21. [CrossRef]

17. Athié, G.; Candela, J.; Sheinbaum, J.; Badan, A.; Ochoa, J. Yucatan Current variability through the Cozumel and Yucatan channels. *Cienc. Mar.* **2011**, *37*, 471–492. [CrossRef]

18. Carrillo, L.; Johns, E.; Smith, R.; Lamkin, J.; Largier, J. Pathways and Hydrography in the Mesoamerican Barrier Reef System Part 1: Circulation. *Cont. Shelf Res.* **2015**, *109*, 164–176. [CrossRef]

19. Orhan, K.; Mayerle, R.; Pandoe, W.W. Assesment of Energy Production Potential from Tidal Stream Currents in Indonesia. *Energy Procedia* **2015**, *76*, 7–16. [CrossRef]

20. Ghefiri, K.; Garrido, A.; Rusu, E.; Bouallègue, S.; Haggège, J.; Garrido, I. Fuzzy Supervision Based-Pitch Angle Control of a Tidal Stream Generator for a Disturbed Tidal Input. *Energies* **2018**, *11*, 2989. [CrossRef]

21. Encarnacion, J.; Johnstone, C. Preliminary Design of a Horizontal Axis Tidal Turbine for Low-Speed Tidal Flow. In Proceedings of the 4th Asian Wave and Tidal Energy Conference, Taipei, Taiwan, 9–13 September 2018.

22. Chávez, G.; Candela, J.; Ochoa, J. Subinertial flows and transports in Cozumel Channel. *J. Geophys. Res. Ocean.* **2003**, *108*. [CrossRef]

23. Ochoa, J.; Candela, J.; Badan, A.; Sheinbaum, J. Ageostrophic fluctuations in Cozumel channel. *J. Geophys. Res. C Ocean.* **2005**, *110*, 1–16. [CrossRef]

24. Abascal, A.J. Analysis of flow variability in the Yucatan Channel. *J. Geophys. Res.* **2003**, *108*, 3381. [CrossRef]

25. Cetina, P.; Candela, J.; Sheinbaum, J.; Ochoa, J.; Badan, A. Circulation along the Mexican Caribbean coast. *J. Geophys. Res. C Ocean.* **2006**, *111*. [CrossRef]

26. Kjerfve, B. Tides of the Caribbean Sea. *J. Geophys. Res.* **1981**, *86*, 4243. [CrossRef]

27. APIQroo. *Manifestación de Impacto Ambiental-Modalidad Particular*; Proyecto Marina Cozumel: Carretera Costera, Mexico, 2018.

28. INEGI. *Censo y Conteos de Población y Vivienda*; Instituto Nacional de Estadística y Geografía: Quintana Roo, Mexico, 2018.

29. SENER-World Bank-ESMAP. *Evaluación Rápida del uso de Energía, Cozumel, Quintana Roo, México*; Technical Report; Secretaría de Energía (SENER), World Bank, Programa de Asistencia para la Gestión del Sector de Energía (ESMAP): Mexico City, Mexico, 2015.

30. SEDETUR. Indicadores Turísticos 2017. Available online: https://www.qroo.gob.mx/sedetur/indicadores-turisticos (accessed on 13 March 2019).

31. Palafox-Muñoz, A.; Zizumbo-Villarreal, L. Distribución territorial y turismo en Cozumel, Estado de Quintana Roo, México. *Gestión Turística* **2009**, *11*, 69–88. [CrossRef]

32. DOF. Decreto por el que se Pretende Declarar Como Área Natural Protegida con el Carácter de Reserva de la Biosfera a la Región Conocida Como Caribe Mexicano. Available online: http://dof.gob.mx/nota_detalle.php?codigo=5464450&fecha=07/12/2016 (accessed on 13 March 2019).

33. DOF. Decreto por el que se Declara Área Natural Protegida, con el Carácter de Area de Protección de Flora y Fauna, la Porción norte y la Franja Costera Oriental, Terrestres y Marinas de la Isla de Cozumel, Municipio de Cozumel, Estado de Quintana Roo. Available online: http://www.dof.gob.mx/nota_detalle.php?codigo=5270007&fecha=25/09/2012 (accessed on 13 March 2019).

34. DOF. Decreto por el que se Declara Área Natural Protegida, con el Carácter de Parque Marino Nacional, la zona Conocida Como Arrecifes de Cozumel. Available online: http://dof.gob.mx/nota_detalle.php?codigo=4892806&fecha=19/07/1996 (accessed on 13 March 2019).

35. Red Nacional de Sistemas Estatales. *Áreas Naturales Protegidas—Decretos de ANPs Quintana Roo*. Available online: https://www.anpsestatales.mx/anps.php?tema=3&estado=25 (accessed on 13 March 2019).

36. Martínez, S.; Carrillo, L.; Marinone, S. Potential connectivity between marine protected areas in the Mesoamerican Reef for two species of virtual fish larvae: Lutjanus analis and Epinephelus striatus. *Ecol. Indic.* **2019**, *102*, 10–20. [CrossRef]

37. Alvera-Azcárate, A.; Barth, A.; Weisberg, R.H. The surface circulation of the Caribbean Sea and the Gulf of Mexico as inferred from satellite altimetry. *J. Phys. Oceanogr.* **2009**, *39*, 640–657. [CrossRef]

38. Rousset, C.; Beal, L.M. Observations of the Florida and Yucatan Currents from a Caribbean cruise ship. *J. Phys. Oceanogr.* **2010**, *40*, 1575–1581. [CrossRef]

39. TELEDYNE Marine. RiverPro ADCP -RD Instruments-. Available online: http://www.teledynemarine.com/riverpro-adcp?ProductLineID=13 (accessed on 12 March 2019).

40. Secretaría de Marina. *Catalogo de Cartas y Publicaciones Náuticas*; Secretaría de Marina, Mexico City, Mexico, 2019; p. 39.

41. The SciPy community. Optimization (scipy.optimize) Available online: https://docs.scipy.org/doc/scipy/reference/tutorial/optimize.html (accessed on 12 March 2019).

42. Shen, W.Z.; Mikkelsen, R.; Sørensen, J.N.; Bak, C. Tip loss corrections for wind turbine computations. *Wind Energy* **2005**, *8*, 457–475. [CrossRef]

43. Manwell, J.F.; McGowan, J.G.; Rogers, A.L. *Wind Energy Explained: Theory, Design and Application*; John Wiley & Sons, Ltd.: Chichester, UK, 2009;

44. Spera, D. *Wind Turbine Technology: Fundamental Concepts in Wind Turbine Engineering, Second Edition*; ASME: New York, NY, USA, 2009.

45. Frost, C.H.; Evans, P.S.; Harrold, M.J.; Mason-Jones, A.; O'Doherty, T.; O'Doherty, D.M. The impact of axial flow misalignment on a tidal turbine. *Renew. Energy* **2017**, *113*, 1333–1344. [CrossRef]

46. Sutherland, D.; Ordonez-Sanchez, S.; Belmont, M.R.; Moon, I.; Steynor, J.; Davey, T.; Bruce, T. Experimental optimisation of power for large arrays of cross-flow tidal turbines. *Renew. Energy* **2018**, *116*, 685–696. [CrossRef]

47. Mycek, P.; Gaurier, B.; Germain, G.; Pinon, G.; Rivoalen, E. Experimental study of the turbulence intensity effects on marine current turbines behaviour. Part I: One single turbine. *Renew. Energy* **2014**, *66*, 729–746. [CrossRef]

48. Harding, S.; Bryden, I. Directionality in prospective Northern UK tidal current energy deployment sites. *Renew. Energy* **2012**, *44*, 474–477. [CrossRef]

49. Laws, N.D.; Epps, B.P. Hydrokinetic energy conversion: Technology, research, and outlook. *Renew. Sustain. Energy Rev.* **2016**, *57*, 1245–1259. [CrossRef]

50. Sandoval Vizcaíno, S. Dinámica de corrientes marinas. In *Biodiversidad acuática de la Isla de Cozumel*; Mejía-Ortíz, L.M., Ed.; Universidad de Quintana Roo-Plaza Y Valdés: Mexico City, Mexico, 2007; Chapter 3.

51. Gallrein, A.; Smith, S. *Cozumel: Dive Guide & Log Book*; Underwater Editions: Cozumel, Quintana Roo, Mexico, 2003.

52. Muckelbauer, G. The shelf of Cozumel, Mexico: Topography and organisms. *Facies* **1990**, *23*, 201–239. [CrossRef]

53. Palafox-Muñoz, A.; Segrado-Pavón, R. Capacidad de carga turística: Alternativa para el Desarrollo Sustentable de Cozumel. *Tur. Desenvolv.* **2008**, *10*, 109.

54. Ordonez-Sanchez, S.; Porter, K.; Frost, C.; Allmark, M.; Johnstone, C.; O'Doherty, T. Effects of Wave-Current Interactions on the Performance of Tidal Stream Turbines. In Proceedings of the 3rd Asian Wave and Tidal Energy Conference, Singapore, 24–28 October 2016.

55. Irena. *Innovation Outlook: Offshore Wind*; Technical Report; International Renewable Energy Agency: Abu Dhabi, UAE, 2016.

56. Vennell, R.; Funke, S.W.; Draper, S.; Stevens, C.; Divett, T. Designing large arrays of tidal turbines: A synthesis and review. *Renew. Sustain. Energy Rev.* **2015**, *41*, 454 – 472. [CrossRef]

57. Blackmore, T.; Myers, L.E.; Bahaj, A.S. Effects of turbulence on tidal turbines: Implications to performance, blade loads, and condition monitoring. *Int. J. Mar. Energy* **2016**, *14*, 1–26. [CrossRef]

58. Nevalainen, T.M. The Effect of uNsteady Sea Conditions on Tidal Stream Turbine Loads and Durability. Ph.D. Thesis, University of Strathclyde, Glasgow, Scotland, 2016.

59.   Liu, Y.; Yu, S.; Zhu, Y.; Wang, D.; Liu, J. Modeling, planning, application and management of energy systems for isolated areas: A review. *Renew. Sustain. Energy Rev.* **2018**, *82*, 460–470. [CrossRef]

60.   Mendoza-Vizcaino, J.; Sumper, A.; Galceran-Arellano, S. PV, wind and storage integration on small islands for the fulfilment of the 50-50 renewable electricity generation target. *Sustainability* **2017**, *9*, 905. [CrossRef]

61.   Mendoza-Vizcaino, J.; Sumper, A.; Sudria-Andreu, A.; Ramirez, J.M. Renewable technologies for generation systems in islands and their application to Cozumel Island, Mexico. *Renew. Sustain. Energy Rev.* **2016**, *64*, 348–361. [CrossRef]